JOURNAL OF AIRCRAFT
Vol. 37, No. 3, May–June 2000

Ground Effect Characteristics of a Two-Dimensional Hypersonic Configuration

Robert E. Bond,* Gary J. Morris,† and John L. Loth‡
West Virginia University, Morgantown, West Virginia 26506-6106

The National Aerospace Plane (NASP) configuration was designed to suit the propulsion needs at hypersonic speeds. Its lower fuselage surface formed the propulsion system with an oblique shock compression ramp, scramjet combustion module, and a single expansion ramp nozzle. To minimize drag, the nose was very thin and the upper surface was nearly flat. How each of these surfaces contribute to its poor low-speed and ground effect performance is demonstrated. This poor performance is characterized by significant power-on lift reduction that is intensified by ejector action while in ground effect. The NASP aerodynamic characteristics were first measured on a three-dimensional model as functions of angle of attack, ground proximity, and thrust coefficient. Then to separate three-dimensional effects from the key problems with this configuration, the tests were repeated with a two-dimensional model based on the fuselage centerline geometry.

Nomenclature

A_p^* = ejector primary choked flow area
A_s = ejector secondary flow area
b = three-dimensional model wing span
C_d = two-dimensional drag coefficient
C_L = three-dimensional lift coefficient (lift/$q_\infty S$)
C_l = two-dimensional lift coefficient
$C_{l\alpha}$ = two-dimensional lift curve slope
C_m = pitching moment coefficient (pitching moment per unit span/$q_\infty c$)
C_p = pressure coefficient
C_T = three-dimensional thrust coefficient (static thrust/$q_\infty S$)
C_t = two-dimensional thrust coefficient
c = two-dimensional model length, referenced to as chord length
h = model height above ground plane, in.
h/b = nondimensional model height above ground plane (three-dimensional models)
h/c = nondimensional model height above ground plane (two-dimensional model)
q_∞ = tunnel dynamic pressure, in. H_2O or psi
Re = Reynolds number
S = three-dimensional model planform area including both wing and fuselage areas
T = static thrust along waterline, lbf
x/c = nondimensional chord position
α = angle of attack, deg

Introduction

A SIGNIFICANT amount of work has been performed to investigate the takeoff/ground effect characteristics of basic hypersonic configurations. As a result of this work, a significant aerodynamic problem was revealed. This is that hypersonic configurations show significant lift loss characteristics when operating in close ground proximity under a power-on condition. The following is a summary of previous work performed to determine these low-speed ground effect characteristics.

Models used for research in this area have all used an array of high-pressure ejectors positioned inside the engine nacelle to provide engine thrust simulation that allowed engine inlet flow simulation as well as high exhaust velocities. Thrust coefficients C_T were defined by normalizing the static model thrust with respect to the tunnel dynamic pressure and the entire model planform area including wing and fuselage. Takeoff thrust values were represented by $C_T = 0.4$.

Preliminary research in this field was conducted by Gatlin[1,2] at NASA Langley Research Center. Gatlin used a generic hypersonic configuration (GHC) model with an overall length of 2.867 m (9.408 ft) mounted in the NASA Langley Research Center 14 × 22 ft subsonic tunnel, as shown in Fig. 1. Tests were run at thrust coefficients from 0.0 to 0.8 and at a unit Reynolds number 1.3×10^6/ft. Ground effect data were taken for a takeoff and approach representative angle of attack chosen to be $\alpha = 12$ deg. Gatlin performed tests to determine the effect of the model height and thrust coefficient on the base configuration lift, drag, and pitching moment. Figure 2 shows the lift coefficient data that were obtained from this study. Gatlin[1] stated that "These data indicate conventional ground effects for the power-off condition as illustrated by increased lift with decreasing model height above the floor. However, this trend reversed as thrust was increased and significant lift losses developed as the model was lowered into ground effect." In addition to this power-on ground effect lift loss, the freestream lift coefficients for the power-on cases were significantly less than those for the power-off condition as shown by lift coefficient data at the maximum model height of $h/b \approx 2.9$.

Further investigation into the ground effect characteristics of hypersonic configurations was performed by Gatlin and Kjerstad.[3] They used a 2.9-m- (9.5-ft-) long (6.5% scale) model of the National Aerospace Plane (NASP) Test Technique Demonstrator (TTD) concept. This model (Fig. 3) was a more accurate representation of a NASP configuration compared to the GHC. It consisted of a dual angle nose ramp, a curved upper surface, and a curved exhaust ramp. This model was tested in the NASA Langley Research Center 14 × 22 ft subsonic tunnel over an angle of attack range of −1 to 27 deg. The freestream dynamic pressure and thrust coefficient ranged from 10 to 80 psf and from 0.0 to 0.8, respectively, although most data were taken with $q_\infty = 40$ psf with a corresponding Reynolds number of 1.2×10^6/ft. Because a 10-deg angle of attack was chosen to represent a takeoff condition, most of the ground effect data were obtained at this angle. The ground effect characteristics for the base TTD geometry were obtained by the use of a fixed ground plane. These data included the lift, drag, and pitching moment coefficients as a function of model height. The lift coefficient data obtained are shown in Fig. 4. It can clearly be seen that, as the model height is reduced and a power-on condition exists, the lift

Received 21 October 1998; revision received 15 May 1999; accepted for publication 19 November 1999.

*Research Assistant Professor, College of Engineering and Mineral Resources, Department of Mechanical and Aerospace Engineering. Member AIAA.

†Associate Professor, College of Engineering and Mineral Resources, Department of Mechanical and Aerospace Engineering. Member AIAA.

‡Professor, College of Engineering and Mineral Resources, Department of Mechanical and Aerospace Engineering. Member AIAA.

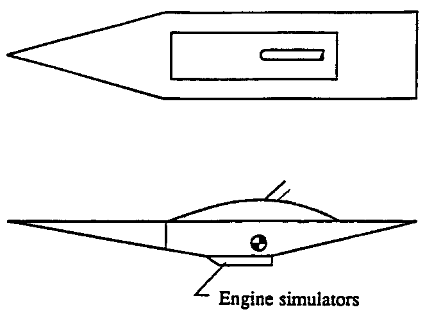

Fig. 1 Generic hypersonic configuration.[2]

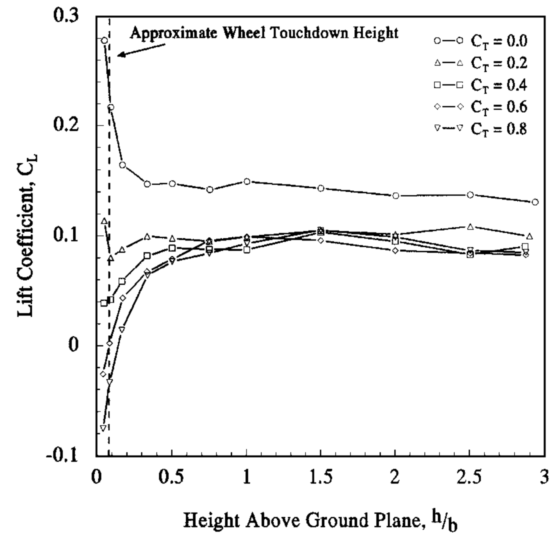

Fig. 2 Effect of *h*/*b* on C_L for GHC[2]: α = 12 deg, various C_T.

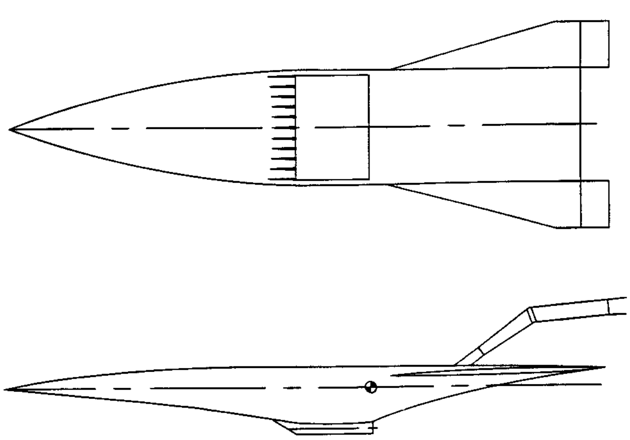

Fig. 3 TTD.[3]

coefficient is significantly reduced. Gatlin and Kjerstad noted that "The rate at which lift is reduced and the magnitude of the power-on lift loss when the configuration is lowered into ground effect are both increased as the thrust coefficient is increased." However, whereas the lift loss is greatest for the C_T =0.8 case, it also has the largest freestream lift coefficient. These effects tend to make the lift coefficients nearly the same for all thrust coefficients when the model is at the approximate wheel touchdown height of h/b =0.05.

The final work that will be discussed here is that of Smith[4] and Smith et al.[5] at West Virginia University (WVU). A model was investigated with an overall length of 1.52 m (5 ft), based on the NASP display model version 2 (Fig. 5) (Ref. 6), mounted in the WVU 6 ×4 ft low-speed tunnel. Figure 6 shows ground effect lift coefficient data taken for this model for thrust coefficients from C_T =0.0 to 0.6. Figure 6 shows that it was found[4,5] that at a 10-deg angle of attack the lift coefficient initially increased as the model was lowered from h/b of 2 to 0.5 for all thrust coefficients. When the model was lowered farther, the lift coefficient remained relatively constant for C_T =0.0 and 0.2, and there was a significant decrease in lift coefficient for thrust coefficients of 0.4 and 0.6.

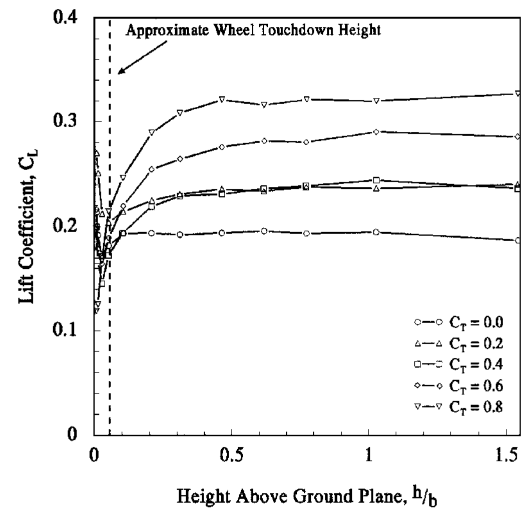

Fig. 4 Effect of *h*/*b* on C_L for NASP TTD[3]: α = 10 deg, various C_T.

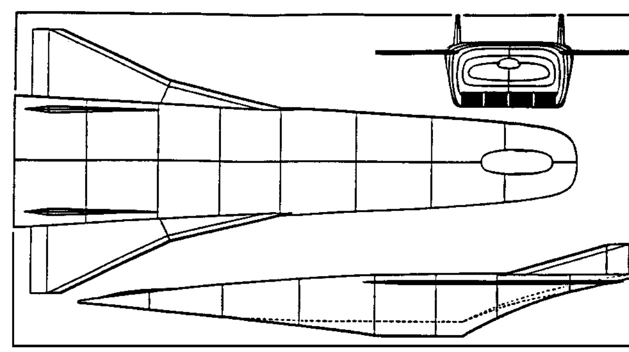

Fig. 5 NASP schematic.[6]

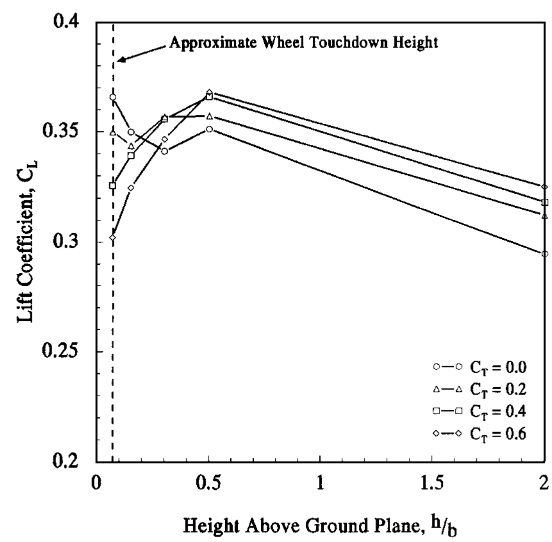

Fig. 6 Effect of *h*/*b* on C_L for display NASP configuration[4,5]: α = 10 deg, various C_T.

The purpose of the present investigation is to determine how the NASP geometrical aspects such as the thin leading nose, near flat upper surface, the shock compression inlet flow ramp and the external expansion ramp nozzle contribute to the ground effect lift loss characteristics. The three-dimensional nature of the models previously tested complicates the flowfield and makes it harder to determine which geometry aspects of the NASP configuration are primarily responsible for its ground effect aerodynamic characteristics. Therefore, it was decided to test a two-dimensional model based on the centerline cross section of the NASP display model version 2. This model provides a detailed surface pressure distribution with a reasonable number of pressure taps and correlation with two-dimensional computational fluid dynamics (CFD) model flowfield predictions. The flow entrainment and separation zones clearly demonstrate the influence the NASP fuselage geometry has on the observed aerodynamic in ground effect performance.

Experimental Apparatus

The basis for the model used for this research was the NASP display model version 2 (Ref. 7). The cross section of the two-dimensional model (Fig. 7), was based on the centerline dimensions of this configuration. The wind-tunnel model was designed with a chord length of 50.8 cm (20 in.) and a span of 81.3 cm (32 in.), which allowed the model to completely span the test section to approximate two-dimensional flow.

Experimental tests were run using this model in the WVU (32 × 45 in.) subsonic wind tunnel (Fig. 8). Data were taken at a dynamic pressure of 311 Pa (6.5 psf), which yielded a $Re = 7.25 \times 10^5$ based on the model chord. The average freestream turbulence intensity when operating under these conditions was found to be 0.215% with a standard deviation of 0.075 as measured using a hot-film anemometer in the empty test section. Using this model, the tunnel blockage was found to range from 5.2% to a maximum of 11.1% depending on angle of attack.

The model thrust was produced by using a high-pressure ejector system located in the model nacelle (Fig. 9). This system was powered by 32 choked nozzles with throat diameters of 3.2 mm (0.126 in.). These nozzles were located at the inlet of the nacelle, which was used as a constant area mixing chamber. Based on this geometry, the ejector system had a secondary to primary area ratio of $A_s / A_p^* = 40.8$. Similar to the previously tested three-dimensional configuration, the static thrust levels produced by this system were

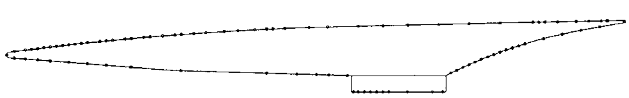

Fig. 7 Cross section of two-dimensional NASP model including pressure tap locations.

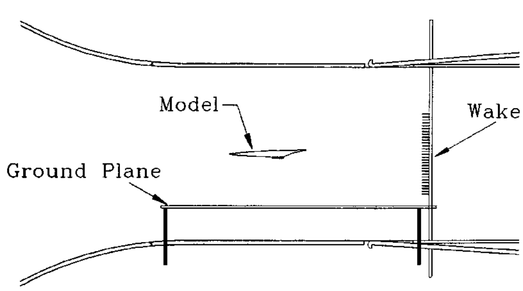

Fig. 8 Wind tunnel test section including model, ground plane, and wake rake.

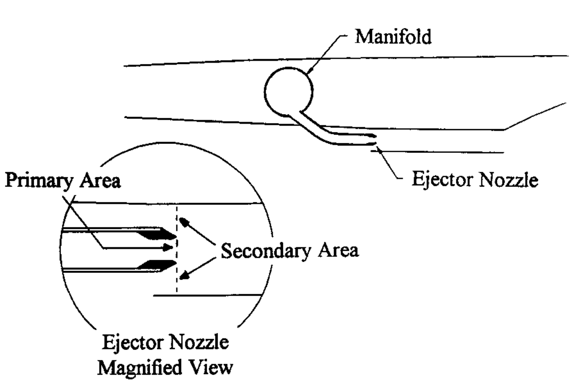

Fig. 9 Model cross section showing ejector system and flow areas.

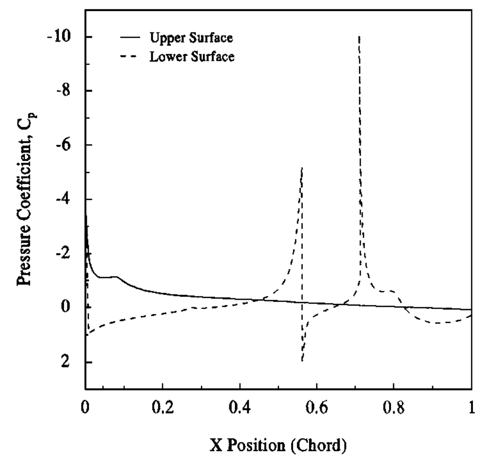

Fig. 10 CFD predicted surface C_p data: $\alpha = 10$ deg, $C_t = 0.4$.

used in the determination of the operational thrust coefficient as given by

$$C_t = \frac{(T/\text{span})_{\text{static}}}{q_\infty c} \tag{1}$$

Normal force and pitching moment coefficients were calculated from model static pressure distributions. These distributions were obtained by measuring the static pressure at 89 independent static pressure taps placed along the model centerline. To minimize the error associated with approximating the continuous pressure distribution with measurements at discrete points, these taps were placed based on a CFD predicted representative pressure distribution, as shown in Fig. 10. The resulting pressure tap locations are shown in Fig. 7. These CFD results were generated using FLUENT version 4.32 with a 25,000 cell grid.

Drag data were obtained through the use of the momentum deficit method, appropriately modified to account for the mass addition of the thrust simulation ejector system. The test section inflow was measured empty prior to model installation and found to be highly uniform. Wake profile data were obtained using a custom-built, two-position, 29 pitot tube wake rake located 1.5 chord lengths downstream of the model trailing edge (Fig. 8). When the ground plane was installed, the measured wake profile was modified to remove the effect of the ground plane boundary layer.

Ground effect data were taken with the use of a variable position 6-ft-long ground plane (Fig. 8). The ground plane spacing was varied by moving the ground plane nearer or farther from the model through the use of four screw jacks. Out of ground effect data were taken with the ground plane removed from the test section to minimize wall effects. Because of the complicated aerodynamic interactions between the boundary layer developed on the stationary ground plane and the model, no attempt was made to remove its affect from the pressure, lift, or pitching moment data. However, as already discussed, the ground plane boundary-layer profile was not included when determining drag coefficient data from the model wake measurements.

Experimental Results

The objective of this research was to characterize the origin of the ground effect aerodynamics of a two-dimensional model of the NASP with thrust simulation.

The results of this investigation were all obtained at the maximum practical Reynolds number of approximately 7.25×10^5 based on the model chord. This value most closely approximates the Reynolds numbers used in the literature; however, is orders of magnitude lower than the Reynolds number at which the proposed NASP would operate.

The coefficients reported and graphically displayed in the following sections were actual measured or computed data. Because these data were taken to achieve a basic understanding of the effect of ground proximity on a two-dimensional hypersonic configuration, they were not Reynolds number corrected to represent actual expected flight conditions. The total uncertainty associated with the presented data are similar for all of the data and, as such, are only shown on the first plot of each type. Additionally, to approximate more closely free-flight data, these data should be corrected for tunnel blockage effects using the procedure outlined by Allen and Vincenti[8] or equivalent. Although this was not done for this paper, these corrections are expected to change the data by less than 10%.

Out of Ground Effect Data

Before investigating the ground effect characteristics of the two-dimensional model, it was important to first quantify the out of ground effect characteristics of this configuration. The first parameter investigated was the lift coefficient and its behavior as a function of both the angle of attack and thrust coefficient, plotted in Fig. 11. The zero thrust curve in Fig. 11 includes error bars representing the average lift coefficient uncertainty that applies to all of the data shown and, as such, was only included for one curve. From these lift coefficient data, it was evident that the overall lift coefficient, at any given angle of attack, reduced with increasing thrust coefficient. The corresponding change in pressure distribution on the surface of the model is shown in Fig. 12 for $C_t = 0.0$ and 0.6 at $\alpha = 10$ deg, with errors on the order of the symbol size. These data indicate the formation of two significant low-pressure regions on the lower surface of the model, one located just upstream of the engine intake and one downstream of the engine exhaust. Additionally, there was a reduction in suction on the upper surface when thrust was applied. This reduction in sectional lift coefficient C_l with increasing sectional thrust coefficient C_t became less significant with increasing angle of attack to the point, at $\alpha = 15$ deg, where the thrust coefficient had little effect on C_l. This behavior was due to the increased lift component of the thrust with increasing angle of attack.

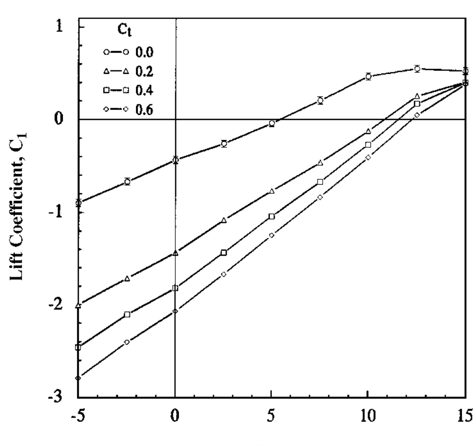

Fig. 11 Effect of angle of attack on lift coefficient for two-dimensional configuration.

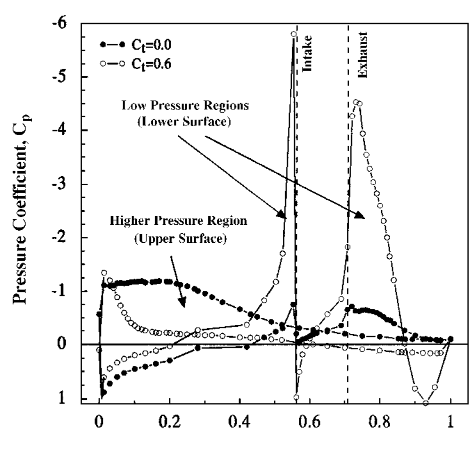

Fig. 12 Comparision of C_p distribution for C_t = 0.0 and 0.6 for two-dimensional configuration: α = 10 deg.

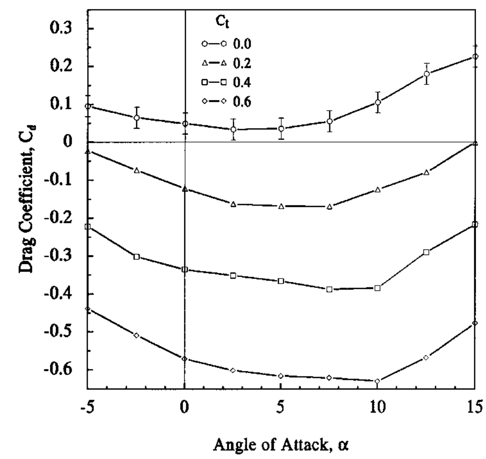

Fig. 13 Effect of angle of attack on drag coefficient for two-dimensional configuration.

Also noted from Fig. 11 was the effect of thrust coefficient on the lift curve slope. For the case of zero thrust, the lift curve slope was $C_{l\alpha} = 1.64\,\pi$, substantially less then the theoretical airfoil maximum slope of 2π, but not suprising because this model experiences some flow separation at nearly all angles of attack. This slope increased to 2.40π at $C_t = 0.2$ and as high as $1\frac{1}{2}$ times the theoretical maximum, or 3.03π, at $C_t = 0.6$. This increase, beyond the unpowered lift theoretical maximum, was due to the increase in simulated vertical engine thrust component with increasing angle of attack.

Interestingly, most of the data in Fig. 11 lie below $C_l = 0$, even at small positive angles of attack with zero thrust. This was due to two effects, the first of which was due to the use of the waterline to define the angle of attack. This waterline passed through the leading edge of the model, but was located significantly lower than the trailing edge. When compared to the aerodynamic angle of attack, as defined by the leading and trailing edges, the waterline angle of attack would yield a value approximately 5 deg larger. Because of this, the data at $\alpha = 5$ deg in Fig. 11 represent data referenced to $\alpha = 0$ deg based on the aerodynamic angle of attack. The second, less significant effect, was due to the model having a slight negative camber, thus yielding a slight negative lift coefficient at zero aerodynamic angle of attack. This effect can be seen by considering the 5-deg angle of attack data, where the aerodynamic angle of attack was approximately zero.

The final characteristic noted from Fig. 11 was the occurrence of airfoil stall. This point is most easily noted for the zero thrust curve, where the lift coefficient falls with increasing angle of attack from 12.5 to 15 deg. This point was not as evident when engine thrust was simulated; however, it was noted as a decrease in the lift curve slope at the same 12.5-deg angle of attack. Flow visualization, using small tufts located on the model upper surface, supported this conclusion. Based on these tufts, it was noted that only a small separation bubble existed near the leading edge at $\alpha = 10$ deg, but massive flow separation areas existed over the entire model upper surface at $\alpha = 12.5$ deg.

The drag coefficient data are plotted as a function of both angle of attack and thrust coefficient in Fig. 13. Note that these data, obtained through the use of the momentum deficit method, included the effect of thrust simulation. As such, many of the data lie below the zero drag line, indicating the point at which the airframe drag equals the thrust. As was the case for the lift coefficient data, error bars representing the average uncertainty in the drag coefficient data are included for the zero thrust case. Once again, these error bars apply to all of the data in Fig. 13, but for clarity were only plotted for this single curve.

By the study of the data in Fig. 13, it was noted that the drag coefficient curve for each individual thrust coefficient appeared similar in trends and differed approximately by the change in thrust coefficient. These curves were similar in that they had minimum values at midrange angles of attack with increasing values at the angle-of-attack limits. Note, however, that the location of the minimum drag point varied with thrust coefficient. This change was from a drag minimum at $\alpha = 2.5$ deg with zero thrust to minimum value at $\alpha = 10$ deg with thrust coefficients of 0.4 and 0.6. This shift in drag minima may have been due to the thrust simulation exhaust not leaving the model exactly parallel to the waterline, but with a slight upward angle. This would cause the effective thrust, parallel to the freestream, to increase slightly with angle of attack until this flow was parallel with the freestream. Although no quantitative data were acquired on this flow angle, this effect would explain the shift in minimum drag as a function of angle of attack.

When studying the decrease in model drag with increasing thrust coefficient, it would be expected that these data would differ by approximately the negative of the thrust coefficient. Although this was the case for these data, there were points where this change in drag was greater than the thrust coefficient. The case of $\alpha = 10$ deg, with $C_t = 0.0$ and 0.6, was a good example of this. For this case, an increase of 0.6 in thrust coefficient yielded a change in drag coefficient of $\Delta C_d = -0.734$, indicating significant thrust augmentation. This characteristic could be due to the effect of the angle of the exhaust flow. Because the thrust coefficient was defined by the thrust parallel to the waterline, if the exhaust vector was not also parallel to this line, the net thrust would be greater than the value used for the thrust coefficient. This characteristic was the same as that discussed concerning the location of the minimum drag point. The largest thrust augmentation occurred at the same angle of attack, $\alpha = 10$ deg, as the minimum drag point in the $C_t = 0.6$ data. This indicates that the exhaust vector is angled approximately 10 deg from the waterline.

The pitching moment data (Fig. 14) showed a significant increase in nose-up pitching moment with increasing thrust coefficient. This dramatic effect was due to the low-pressure regions on the lower surface formed aft of the quarter-chord point when thrust was added (see Fig. 12), as well as the thrust vector being located below the model centerline. The error bars shown for the zero thrust data in Fig. 14 are average values and are applicable to all of the pitching moment data.

The C_m data (Fig. 14) showed a relatively flat profile for zero thrust coefficient, indicating neutral static stability in pitch. When thrust was introduced, the curves became markedly curved with maxima around the $\alpha = 2.5$–5.0 deg range. These data indicate a stability-induced tendency toward these angles of attack.

Ground Effect Data

Ground effect data were obtained at a takeoff representative angle of attack of 10 deg, which corresponded with the related studies noted in the literature.

The lift coefficient data were plotted as a function of the nondimensional ground plane spacing in Fig. 15. In Fig. 15, the out of ground effect data are represented at $h/c = 1$, which was the approximate spacing between the model and the test section wall. For thrust coefficients of 0.0 and 0.2, the effect of lowering the model into ground effect acts to increase the lift coefficient. At thrust coefficients in excess of 0.2, the ground effect characteristics changed markedly. For C_t values of 0.4 and 0.6, a strong lift loss was encountered as the model was lowered into ground effect. This increased lift loss with increasing thrust coefficient was similar to that experienced for the three-dimensional models (Figs. 2, 4, and 6). At a thrust coefficient of 0.6, the lift coefficient for the two-dimensional model had a maximum change of 208%, from $C_l = -0.410$ to -1.263 at $h/c = 0.075$, which reduced to a 145% change at $h/c = 0.15$ for the 0.4 thrust coefficient case.

To illustrate the effect of ground plane spacing on the model surface pressure distribution, Fig. 16 was constructed. Plotted in Fig. 16 are the data obtained at minimum and maximum ground plane spacings ($h/c = 0.075$ and 1) with the model operating at the maximum tested thrust coefficient ($C_t = 0.6$). From Fig. 16, the cause of the ground effect lift loss is readily identifiable. When the upper surface of the model is considered, it can be seen that close ground proximity is accompanied by a slight increase in upper surface suction, acting to increase the overall lift coefficient. However, the effect of ground plane spacing on the lower surface pressure distribution is far more dramatic. On this surface, three strong low-pressure regions are significantly enhanced when the model is in close ground proximity. These regions are located just upstream of the engine intake, on the engine nacelle, and, the primary region, just downstream of the engine exhaust location. The combination of the strong suction regions formed on the lower surface overwhelms the sightly increased suction on the upper surface to reduce dramatically the overall section lift coefficient. Similar pressure distribution changes were noted at lower thrust coefficients and angles of attack where the ground effect lift loss characteristic was present.

The ground effect drag data (Fig. 17) all show similar ground effect characteristics. Each of the thrust coefficient curves showed

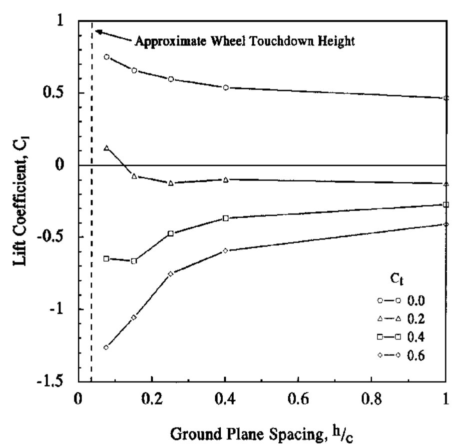

Fig. 15 Effect of ground plane spacing on lift coefficient for two-dimensional configuration: α = 10 deg.

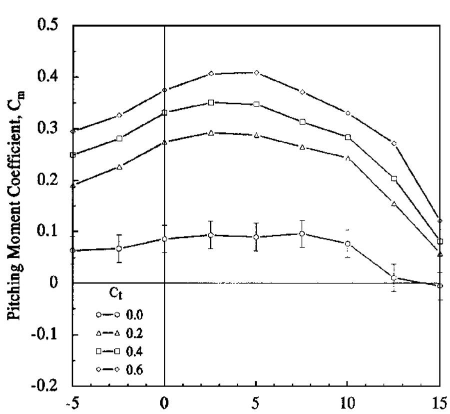

Fig. 14 Effect of angle of attack on pitching moment coefficient for two-dimensional configuration (quarter chord reference).

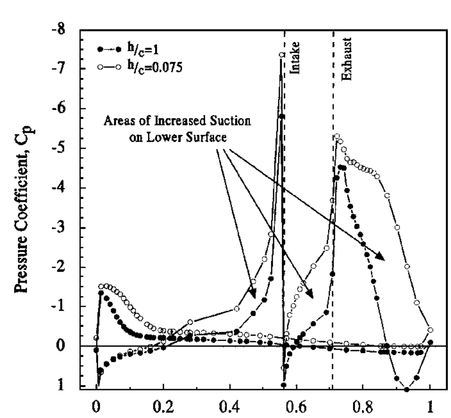

Fig. 16 Comparision of C_p distribution for h/c = 1 and h/c = 0.075 for two-dimensional configuration: α = 10 deg, C_t = 0.6.

an increase in drag when the ground plane was approached. For the larger thrust coefficients, $C_t = 0.4$ and 0.6, the drag data remained relatively flat until the $h/c = 0.15$ point was reached. This was the approximate point at which the flow blockage was shown to dominate in the lift coefficient data. Based on this, it was inferred that this increase in drag coefficient was primarily due to the blockage effect that increased the pressure on the slightly forward facing, lower surface of the model.

The effect of ground proximity on the pitching moment coefficient is shown in Fig. 18. From these data, it was noted that, for zero thrust coefficient, a reduction in the ground plane spacing had a subsequent reduction in the nose-up pitching moment. However, when thrust was added, the effect was reversed. The pitching moment increased with reducing ground plane spacing until the model was in very close ground proximity where blockage becomes significant.

To identify similarities between the two-dimensional ground effect lift coefficient data and those of a three-dimensional configuration, Fig. 19 was constructed. Figure 19 contains takeoff and landing representative ground effect lift coefficient data for both the two-dimensional model used for this research and the three-dimensional GHC tested by Gatlin.[2] The GHC was chosen for this comparison because this model had no wings, flaps, or tail surfaces and, as such, was believed to be the most suitable for this comparison. From Fig. 19, it is evident that, for the case of zero thrust, both configurations showed similar ground effect lift increases with reductions in ground plane spacing. It was also noted that the two-dimensional model showed significantly higher zero thrust lift coefficients than did the three-dimensional model. When takeoff thrust was applied, both models experienced an overall reduction in lift coefficient throughout the ground plane spacing range; however, this thrust-induced lift loss was much more significant for the two-dimensional configuration. Additionally, both configurations showed a reversal in ground effect characteristic from a lift increase to a lift loss with reductions in ground plane spacing. Although both of these models showed similar trends, it was noted that all of the characteristics observed in the three-dimensional model data were significantly enhanced in those for the two-dimensional model.

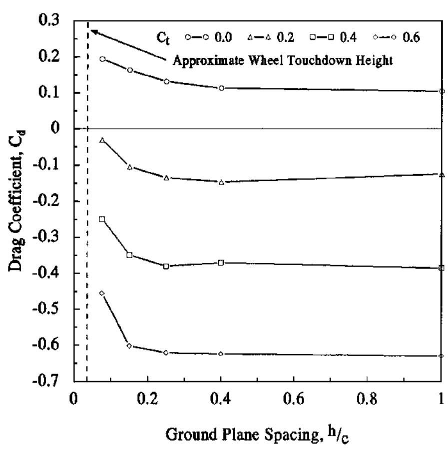

Fig. 17 Effect of ground plane spacing on drag coefficient for two-dimensional configuration: $\alpha = 10$ deg.

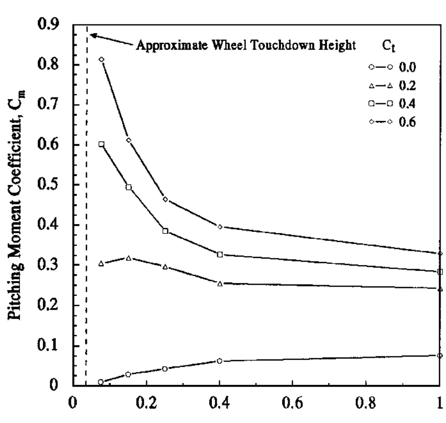

Fig. 18 Effect of ground plane spacing on pitching moment coefficient for two-dimensional configuration: $\alpha = 10$ deg.

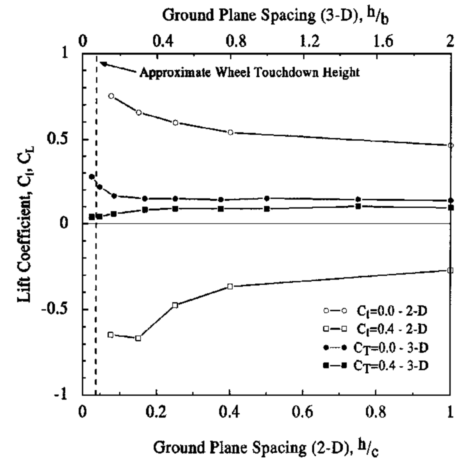

Fig. 19 Comparison of two-dimensional configuration ($\alpha = 10$ deg) and three-dimensional GHC ($\alpha = 12$ deg) ground effect lift coefficient data.

Conclusions

The trends in power-on ground effect lift loss characteristics observed for three-dimensional models could be reasonably reproduced using two-dimensional models of similar cross section. Two-dimensional configurations are much easier to construct, pressure test, and simulate computationally.

Model pressure distributions allowed for the identification of the single expansion ramp nozzle as the region primarily responsible for ground effect lift loss characteristics. This research indicates that to significantly improve ground effect performance of a hypersonic configuration, modifications must be made to reduce the effect of high-velocity exhaust on the lower surface of the model.

Acknowledgment

This research was supported under NASA/West Virginia University/National Aerospace Plane Grant NAG1-1584, with David Reubush, Grant Monitor, Hyper-X Stage Separation Manager, Hyper-X Program Office, NASA Langley Research Center.

References

[1]Gatlin, G. M., "Low-Speed Aerodynamic Characteristics of a Powered NASP-Like Configuration in Ground Effect," Society of Automotive Engineers, TP 892312, Sept. 1989.

[2]Gatlin, G. M., "Ground Effects on the Low-Speed Aerodynamics of a Powered, Generic Hypersonic Configuration," NASA TP 3092, 1991.

[3]Gatlin, G. M., and Kjerstad, K. J., "Low-Speed Longitudinal Aerodynamic Characteristics of a Powered National Aero-Space Plane Test Technique Demonstrator Configuration In and Out of Ground Effect," NASP TP 1012, Feb. 1994.

[4]Smith, G., "Aerodynamic Coefficients of a Hypersonic NASP Model in Ground Effect," M.S. Thesis, West Virginia Univ., Morgantown, WV, 1996.

[5]Smith, G., Bond, R., Loth, J., and Morris, G., "NASP Take-Off Lift Loss Alleviation," AIAA Paper 97-0296, Jan. 1997.

[6]Taylor, J. W. R., *Jane's All The World's Aircraft 1991–92*, Jane's Information Group, Ltd., Alexandria, VA, 1989, pp. 455, 456.

[7]Romero, J. M., "Configuration Layout, NASP Display Model Version 2," Preliminary Design Drawing FW9010009A, General Dynamics, Fort Worth Div., Fort Worth, TX, Nov. 1990.

[8]Allen, H. J., and Vincenti, W. G., "Wall Interference in a Two-Dimensional Flow Wind Tunnel, with Consideration of the Effect of Compressibility," National Advisory Committee for Aeronautics, Rept. 782, 1944.